

Hyperspectral fluorescence microscopy detects autofluorescent factors that can be exploited as a diagnostic method for *Candida* species differentiation

Matthew S. Graus
Aaron K. Neumann
Jerilyn A. Timlin

Hyperspectral fluorescence microscopy detects autofluorescent factors that can be exploited as a diagnostic method for *Candida* species differentiation

Matthew S. Graus,^a Aaron K. Neumann,^{a,*} and Jerilyn A. Timlin^b

^aUniversity of New Mexico, Department of Pathology, 1 University of New Mexico, MSC08 4640, Albuquerque, New Mexico 87131, United States

^bSandia National Laboratories, Department of Bioenergy and Defense Technologies, P. O. Box 5800, MS 0895, Albuquerque, New Mexico 87185, United States

Abstract. Fungi in the *Candida* genus are the most common fungal pathogens. They not only cause high morbidity and mortality but can also cost billions of dollars in healthcare. To alleviate this burden, early and accurate identification of *Candida* species is necessary. However, standard identification procedures can take days and have a large false negative error. The method described in this study takes advantage of hyperspectral confocal fluorescence microscopy, which enables the capability to quickly and accurately identify and characterize the unique autofluorescence spectra from different *Candida* species with up to 84% accuracy when grown in conditions that closely mimic physiological conditions. © The Authors. Published by SPIE under a Creative Commons Attribution 3.0 Unported License. Distribution or reproduction of this work in whole or in part requires full attribution of the original publication, including its DOI. [DOI: [10.1117/1.JBO.22.1.016002](https://doi.org/10.1117/1.JBO.22.1.016002)]

Keywords: *Candida albicans*; *Candida glabrata*; *Candida parapsilosis*; autofluorescence; spectral analysis.

Paper 160325RR received May 23, 2016; accepted for publication Dec. 12, 2016; published online Jan. 5, 2017.

1 Introduction

Candida species are commensal pathogens that usually reside on mucosal surfaces. If given the opportunity, the fungus will transition from a commensal organism to become a pathogen, which can create infections that range from superficial to systemic. *Candida* species are the most common fungal pathogens, with *C. albicans* arising the most often followed by *C. glabrata* and *C. parapsilosis*, respectively.¹⁻⁴ Not only is there a high mortality rate associated with candidiasis but there is also a healthcare cost that can exceed billions of dollars annually.^{1,5-7}

To reduce mortality associated with fungal infections, early and accurate identification is essential. Studies have shown that late and incorrect diagnosis of *Candida* species leads to a significant increase in mortality.^{8,9} There are multiple clinical diagnostic methods used to support candidiasis diagnoses. Regardless of the detection method (e.g., mass spectrometry and polymerase chain reaction), a microbiological culture step is usually required prior to pathogen identification. This culture step can take between 2 and 5 days from receipt of a clinical sample (e.g., blood, catheter tip, sputum, and urine) for microbiological identification. This long time-to-identification can lead to delays in initiation of optimal antimicrobial chemotherapy. Previous studies have shown relatively poor sensitivity of clinical diagnostics for candidiasis, with a 30% to 50% false negative rate for blood cultures in patients with autopsy-confirmed cases of candidiasis.^{10,11} This demonstrates the limitations of both time and reliability of diagnosis for common existing diagnostic approaches for candidiasis.

Cellular autofluorescence has demonstrated potential as a clinical diagnostic method because it is noninvasive and label-free and has the ability to supply morphological and

biochemical information. Studies have shown that autofluorescence emission can be used to detect microbial pathogens, such as *Mycobacterium tuberculosis*¹² and some pathogenic fungi,¹³ whereas other studies have exploited autofluorescence emission to detect cancer cells.^{14,15} Utilizing autofluorescence is possible due to the differences in both structure and biochemistry of the pathogen and/or the biochemical changes in cells and tissue resulting from disease. Recently, fungal pathogens have been shown to emit autofluorescence in the visible spectrum using blue/green excitation wavelengths.¹⁶ We hypothesize that the autofluorescence emission can be used as a means of rapid identification and can be used parallel to traditional methods to provide a guide for appropriate care at an earlier time.

In this study, we use hyperspectral confocal fluorescence microscopy (HCFM) and multivariate spectral analysis methods to resolve multiple autofluorescence spectra in three *Candida* species pathogens. Utilizing these methods, we were able to identify two independent autofluorescence emission spectra in *Candida* species grown under physiologically relevant conditions. The relative abundance of these spectral factors, together with intracellular spatial distribution features, was sufficient to yield species level differentiation in laboratory experiments.

2 Results

We grew lab strain yeasts of *C. albicans*, *C. glabrata*, and *C. parapsilosis* described in Materials and Methods for the purpose of ascertaining if the individual *Candida* species have unique autofluorescence characteristics. In these studies, we initially used three different growth media: yeast extract peptone dextrose (YPD) (a rich fungal medium), Roswell Park Memorial Institute medium (RPMI 1640) with 3-(N-morpholino)propane-sulfonic acid (MOPS), and pooled human serum. The human serum growth condition was chosen for continued experimentation because of its similarity to the growth condition of fungal pathogens in peripheral blood.

*Address all correspondence to: Aaron K. Neumann, E-mail: akneumann@salud.unm.edu

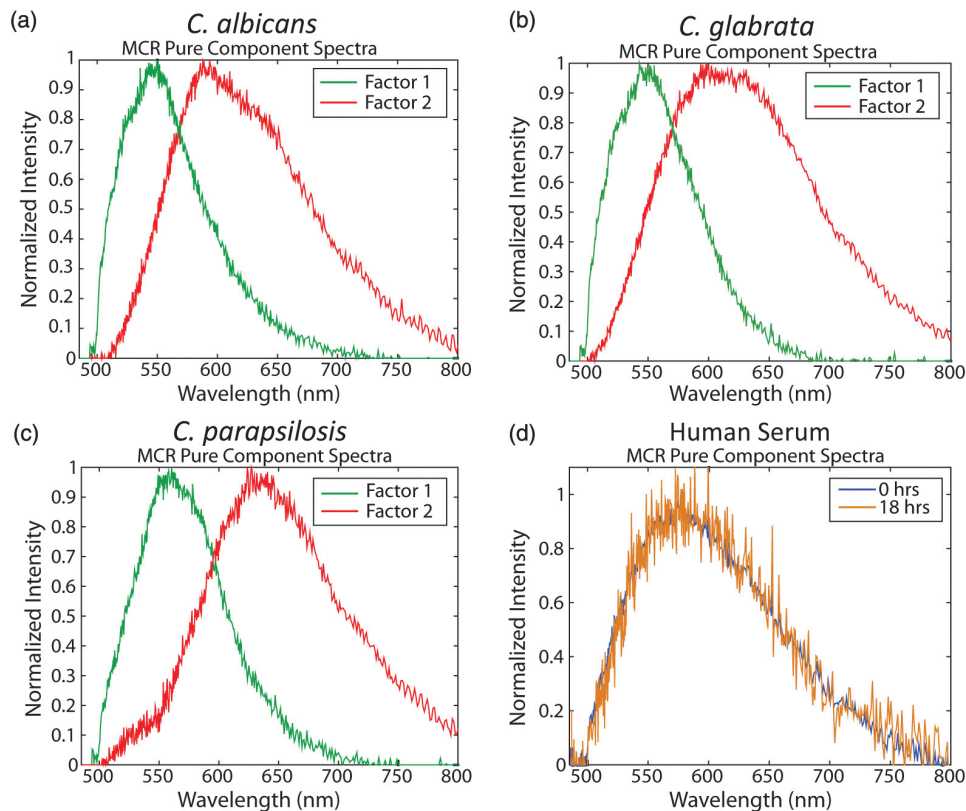


Fig. 1 MCR identified emission spectra of *Candida* species. (a–c) Two emission spectra that were derived from MCR analysis after 16 h of incubation with *Candida* species. (d) Emission spectra of human serum at 0 h incubation and 18 h of incubation to demonstrate that emission factors found in *Candida* samples are not due to emission of human serum. (a–c) Fungal emission spectra are composed from ≥ 80 cells and (d) serum emission spectra composed from 1 sample at 0 h of incubation and 18 h of incubation.

We detected autofluorescence emission from all of the *Candida* species in all growth media. However, there were no significant differences between species grown in YPD and RPMI when looking at the number of spectral factors detected, the shape of the spectral factor, their wavelength of maximum emission, or their relative abundances throughout the fungal cells. In human serum, however, samples exhibited differences in autofluorescence depending on the species. Because this condition most closely matches the nature of clinical samples, we focused our further investigations on autofluorescence components for *Candida* in human serum. The multivariate curve resolution (MCR) analysis resulted in two different emission factors for all species [Figs. 1(a)–1(c)]. Factor 1's spectral shape and peak (550 nm) are very similar across all species, leading to the idea that the three species investigated share a set of common autofluorescent molecules that emit around 550 nm. In contrast, factor 2's spectral shape and peak (600 to 650 nm) vary depending on which species are being observed [Figs. 1(a)–1(c)]. For example, *C. albicans* factor 2 peak is found at 600 nm, *C. parapsilosis* factor 2 peak is found at 650 nm, and, interestingly, *C. glabrata* factor 2 peak is broad (the peak encompasses 600 to 650 nm). When we examined autofluorescent emission from human serum alone, it did not match either factor found in the *Candida* samples and is not an obvious linear combination of the two factors [Fig. 1(d)].

Along with the spectral factors, the MCR analysis also returns concentration maps that indicate the relative abundance

of each spectral factor. To determine if the spatial localizations of autofluorescence emissions were similar, these concentration maps were overlaid to create composite images, where the green and red color channels correspond to the independent concentration map corresponding to spectral factor 1 and 2, respectively. The composite images were then examined to see if the individual factor's emission came from similar spatial localizations. We found that *C. albicans* factors were mostly spatially separated, whereas both *C. glabrata* and *C. parapsilosis* factors were found to be localized in the same general area within the cells. Next, we compared the spatial localization patterns between species and found unique patterns for each species (Fig. 2). In the case of *C. albicans*, we found very small features mostly composed of factor 1 that were on average around $0.42 \mu\text{m}^2$. For *C. parapsilosis*, we observed large features primarily composed of factor 2 that are on average around $1 \mu\text{m}^2$. However, features in *C. glabrata* images contained both factor 1 and factor 2 with an average area around 0.27 and $0.67 \mu\text{m}^2$, respectively. Remarkably, the majority of autofluorescence from *C. parapsilosis* comes from factor 2. Mean factor 2 intensity of the *C. parapsilosis* features was twofold greater than *C. glabrata* features and tenfold greater than *C. albicans* features. Similar trends are also observed when quantifying the other characteristics of *C. parapsilosis* autofluorescence. These differences in autofluorescence emission geometry as well as other autofluorescence characteristics allowed us to create a classifier from the spatial

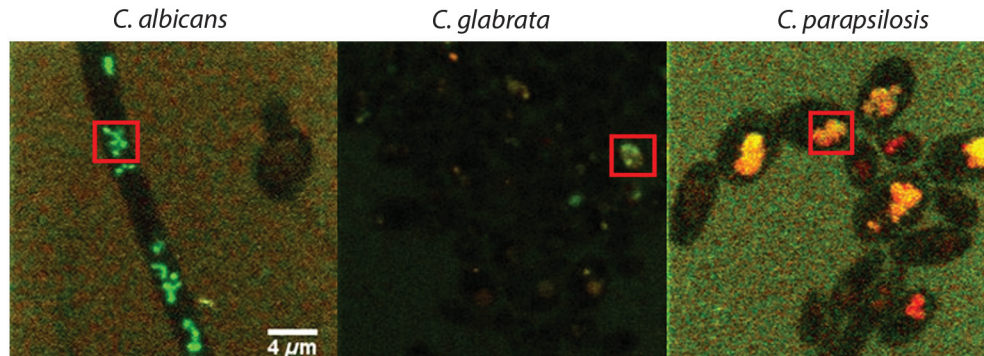
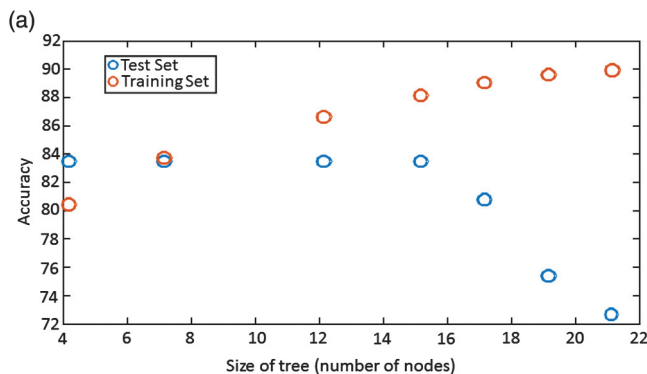


Fig. 2 Representative R-G composite images of two autofluorescence factors of *Candida* species. The green channel reflects factor 1 signal and the red channel reflects factor 2 signal. Red boxes are to highlight autofluorescent feature within the fungal cells. Color channels in each image are scaled independently of each other, using a minimum to maximum scale to enhance visualization. Image size and magnification are the same for all images.

and spectral features of the autofluorescence emission that are unique to individual species.

To create an image diagnostic algorithm based on the autofluorescence emission, we quantified multiple spatial and spectral characteristics of each of the autofluorescence signatures from the feature within the hyperspectral fluorescence images. To validate the accuracy of the classification tree, we measured three statistics for six levels of pruning using the training set (described in Materials and Methods) and plotted the accuracy of both the training set and test set [Figs. 3(a) and 3(b)]. The statistics and accuracy plot revealed some of the less pruned classification trees (i.e., larger classification trees) have a lower true predictive error, demonstrating that the full classification tree may have been overfitting and that the predictions reflected

noise or outliers. The accuracy plot also depicted the pruning level (i.e., size of the classification tree) where the training set and test set diverged. Based on these results, we selected level 4 as the optimal pruning level. From the pruned tree, we were able to achieve 84% accurate species identification from the test set of data [Fig. 3(b)]. We were also able to observe which autofluorescent characteristics were used to construct the classification tree (Fig. 4). Interestingly, in this predictive model, factor 1 autofluorescent characteristics are more important than factor 2 characteristics for predicting the *Candida* species. We then calculated the predictive accuracy for identifying each species in the independent test set. The classification tree was able to predict 75% of *C. albicans* samples accurately, 88% of *C. glabrata* accurately, and 83% of *C. parapsilosis* accurately. On closer inspection of the results, it was found that *C. albicans* was misidentified twice, once with *C. glabrata* and once with *C. parapsilosis*. Whereas *C. glabrata* was found to only be misidentified with *C. parapsilosis* and *C. parapsilosis* misidentified with *C. glabrata*.



(b)

Pruning Level/Number of Nodes	Resubstitution Error (Training Set)	Cross Validation Error (Training Set)	True Predictive Error (Test Set)	Accuracy (Test Set)
Full Tree/21	0.0979	0.2374	0.2703	72.97
Level 1/19	0.1009	0.2136	0.2432	75.68
Level 2/17	0.1068	0.2522	0.1892	81.08
Level 3/15	0.1157	0.2315	0.1622	83.78
Level 4/12	0.1306	0.2344	0.1622	83.78
Level 5/7	0.1602	0.2315	0.1622	83.78
Level 6/4	0.1929	0.2404	0.1622	83.78

Fig. 3 Classification tree pruning. (a) Overfitting decreases the accuracy of the classification tree for the test set. Pruning level for classification tree was chosen by the divergence of the test set and training set, which corresponds with pruning level 4 (i.e., a 12 node classification tree). (b) Table displaying statistics for the different pruning levels of the classification tree. Bold statistics indicate chosen level for prediction analysis of the test set.

3 Discussion

Candida species are well known for their ability to cause morbidity and mortality. It is also known that some species, such as *C. glabrata*, have intrinsic resistances to azole-based antifungal drugs.^{17,18} Due to this, it is important to be able to quickly and accurately identify the pathogenic fungal species prior to administering treatment. The method we describe in this study takes advantage of the spatial and spectral resolution of HCFM. The ability to characterize the unique autofluorescence spectra in the different *Candida* species coupled with their spatial localizations has allowed for species level identification of *Candida* species yeasts grown in conditions that closely mimic pathological conditions and commonly available clinical specimen types.

The serum growth condition was chosen and designed to be a model of growth conditions in blood. Most of the samples assayed for *Candida* in diagnostic reference laboratories are peripheral blood (~96% of specimens in our clinical isolate library) and the remainder are mostly medical devices in intimate contact with central circulation. Serum is a reasonable and tractable model for blood in that it contains all noncellular blood components except clotting factors. It is commonly used to study the response of *Candida* to growth in conditions that mimic growth in systemic circulation. Indeed, *Candida* species are known to respond to growth in serum with

with other technologies would be a worthy subject of future investigation.

In summary, currently deployed fungal species identification methods based on culture can range from 2 to 5 days depending on the method being used, which can cause complications related to delays in treatment. The laboratory investigation conducted demonstrates a 75% prediction accuracy for *C. albicans*, 88% prediction accuracy for *C. glabrata*, and 83% prediction accuracy for *C. parapsilosis* in clinically relevant media. The next step to determine robustness of this method will be to include clinical samples. Our work represents the first step toward developing a label-free method for rapid, culture-free identification of fungal species. If used parallel with traditional methods it could provide a guide for appropriate care at an earlier time and could reduce morbidity and mortality.

4 Methods

4.1 Yeast Growth/Preparation

C. albicans (ATCC, MYA-2876), *C. glabrata* (ATCC, 2001), and *C. parapsilosis* (ATCC, 22019) were grown from glycerol stock, stored at -80°C . Samples were grown in YPD, RPMI-1640 + 0.165M MOPS, or human serum (EMD Millipore, S1) for 16 h at 37°C in an orbital shaker at 250 rpm. Yeast were then put on microscope slides and sealed with nail polish.

4.2 Hyperspectral Confocal Fluorescence Microscopy

A custom built HCFM was used to acquire the autofluorescent emissions from the samples. Previous work describes the methodology for image acquisition using the custom built microscope.²⁵ In summary, a 488-nm laser (Coherent, Inc. Sapphire) and a 60 \times apochromat objective (Olympus Plan Apochromat, NA 1.4) were used to excite fluorescence from a diffraction-limited spot. The laser power was $\sim 80\ \mu\text{W}$ at the entrance to the microscope and the integration time was 0.2 ms/pixel. To detect fluorescent emissions, a prism spectrometer coupled to an electron multiplying charged-coupled device camera (Andor Technologies, Inc., iXon) was used.

4.3 Spectral Analysis

All images were preprocessed to remove known spectral artifacts introduced by the imaging system (cosmic ray spikes, detector offset, and structured dark noise),²⁶ as well as to calibrate the wavelength axis. The resulting individual spectral images were combined into three composite image data sets, one for each *Candida* species. MCR was performed on each of these composite data sets to develop a spectral model that described more than 98% of the spectral variance. The MCR algorithm has been described previously^{27,28} and has demonstrated success in exploratory analysis to identify underlying spectral components from multicomponent biological systems.^{29,30} The MCR results identified near-identical spectral components regardless of the yeast species; therefore, a combined spectral model for all three species was deemed appropriate. This combined model was generated by performing MCR on a combined set of images from all three species and described >96% of the spectral variance in the data. Classical least squares prediction was used to determine the location and abundance of each spectral component in the spectral images. Images corresponding to the location and abundance of individual spectral

components were exported as Tif files for subsequent image processing.

4.4 Classification

Fiji (ImageJ) was used to threshold and quantify features. A threshold of three standard deviations above background intensity was used to extract features for all emission factors. Quantification of features was measured for total and average intensity per feature, average intensity variance per feature, total and average number of features per cell, and total and average area of features describing the nature of the autofluorescence in the cells. The characteristics were then compiled and input into a binary classification tree algorithm. A classification tree analysis was developed in MATLAB[®] using the statistics, and a machine learning toolbox (Mathworks, version 2015a) was then used to create the classification tree and accuracy statistics. To test the performance of the classifier, we divided the data into a training group of 337 cells and a test group of 37 cells (composed of 10% of each species population). To validate the accuracy of the classification tree, we measured three statistics: cross validation error, resubstitution error, and the true predictive error for six levels of tree pruning using the training set. To calculate the true error of prediction, the number of misclassifications in the test set was divided by the total number of samples in the training set. All data presented were pooled from triplicate biological replicates of samples.

Disclosures

The authors disclose that there are no financial interests or conflicts of interest.

Acknowledgments

We appreciate the contributions of Michael Wester and the members of the Neumann lab. We also thank Michael Sinclair for use and maintenance of the hyperspectral confocal microscope and Howland D.T. Jones for the MCR software package. This work was supported by National Institutes of Health (NIH) Grant AI007538 (M.S.G), NIH Grant P50GM085273 supporting the Center for Spatiotemporal Modeling of Cell Signaling, NIH Grant R01AI116894 (A.K.N.), and NIH Director's New Innovator Award Program 1-DP2-OD006673-01 (J.A.T.). Sandia National Laboratories is a multiprogram laboratory that is managed and operated by Sandia Corporation, a wholly owned subsidiary of Lockheed Martin Corporation, for the US Department of Energy's National Nuclear Security Administration (contract No. DE-AC04-94AL85000).

References

1. S. Magill et al., "Multistate point-prevalence survey of health care-associated infections," *N. Engl. J. Med.* **370**, 1198–1208 (2014).
2. N. Yapar, "Epidemiology and risk factors for invasive candidiasis," *J. Ther. Clin. Risk Manage.* **10**, 95–105 (2014).
3. S. R. Lockhart, "Current epidemiology of *Candida* infection," *Clin. Microbiol. Newsl.* **36**(17), 131–136 (2014).
4. M. Pfaller and D. Diekema, "Epidemiology of invasive candidiasis: a persistent public health problem," *Clin. Microbiol. Rev.* **20**(1), 133–163 (2007).
5. O. Gudlaugsson et al., "Attributable mortality of nosocomial candidemia, revisited," *Clin. Infect. Dis.* **37**(9), 1172–1177 (2003).
6. F. G. De Rosa et al., "Invasive candidiasis and candidemia: new guidelines," *Minerva Anesthesiol.* **75**(7–8), 453–458 (2009).

7. R. P. Wenzel and M. B. Edmond, "The impact of hospital-acquired bloodstream infections," *Emerg. Infect. Dis.* **7**, 174–177 (2001).
8. M. Morrell, V. Fraser, and M. Kollef, "Delaying the empiric treatment of *Candida* bloodstream infection until positive blood results are obtained: a potential risk factor for hospital mortality," *Antimicrob. Agents Chemother.* **49**(9), 3640–3645 (2005).
9. K. Garey et al., "Time to initiation of fluconazole therapy impacts mortality in patients with candidemia: a multi-institutional study," *Clin. Infect. Dis.* **43**(1), 25–31 (2006).
10. M. Kami et al., "Effect of fluconazole prophylaxis on fungal blood cultures: an autopsy-based study involving 720 patients with haematological malignancy," *Br. J. Haematol.* **117**(1), 40–46 (2002).
11. J. Berenguer et al., "Lysis-centrifugation blood cultures in the detection of tissue-proven invasive candidiasis disseminated versus single-organ infection," *Diagn. Microbiol. Infect. Dis.* **17**(2), 103–109 (1993).
12. S. Patino et al., "Autofluorescence of mycobacteria as a tool for detection of *Mycobacterium tuberculosis*," *J. Clin. Microbiol.* **46**(10), 3296–3302 (2008).
13. C. Margo and T. Bombardier, "The diagnostic value of fungal autofluorescence," *Surv. Ophthalmol.* **29**(5), 374–376 (1985).
14. I. Miranada-Lorenzo et al., "Intracellular autofluorescence: a biomarker for epithelial cancer stem cells," *Nat. Methods* **11**(11), 1161–1169 (2014).
15. V. Jayaprakash et al., "Autofluorescence-guided surveillance for oral cancer," *Cancer Prev. Res.* **2**(11), 966–974 (2009).
16. J. D. Walsh et al., "Rapid intrinsic fluorescence method for direct identification of pathogens in blood cultures," *MBio* **4**(6), e00865 (2013).
17. Z. Khan et al., "Emergence of resistance to amphotericin B and triazoles in *Candida glabrata* vaginal isolates," *J. Chemother.* **20**, 488–491 (2008).
18. A. Panackal et al., "Clinical significance of azole antifungal drug cross-resistance in *Candida glabrata*," *J. Clin. Microbiol.* **44**(5), 1740–1743 (2006).
19. D. Lowman et al., "Mannan structural complexity is decreased when *Candida albicans* is cultivated in blood or serum at physiological temperature," *Carbohydr. Res.* **346**(17), 2752–2759 (2011).
20. S. Siano and R. Mutharasan, "NADH and flavin fluorescence responses to starved yeast cultures to substrate additions," *Biotechnol. Bioeng.* **34**(5), 660–670 (1989).
21. H. Bhatta and E. M. Goldys, "Characterization of yeast strains by fluorescence lifetime imaging microscopy," *FEMS Yeast Res.* **8**(1), 81–87 (2008).
22. A. Kindzelskii and H. R. Petty, "Fluorescence spectroscopic detection of mitochondrial flavoprotein redox oscillations and transient reduction of the NADPH oxidase-associated flavoprotein in leukocytes," *Eur. Biophys. J.* **33**(4), 291–299 (2004).
23. S. Silva et al., "*Candida glabrata*, *Candida parapsilosis* and *Candida tropicalis*: biology, epidemiology, pathogenicity and antifungal resistance," *FEMS Microbiol. Rev.* **36**(2), 288–305 (2012).
24. G. Borekci et al., "Identification of *Candida* species from blood cultures with fluorescent in situ hybridization (FISH), polymerase chain reaction-restriction fragment length polymorphism (PCR-RFLP) and conventional methods," *Med. J. Trak. Univ.* **27**(2), 183–191 (2009).
25. M. B. Sinclair et al., "Hyperspectral confocal microscope," *Appl. Opt.* **45**(24), 6283–6291 (2006).
26. H. D. T. Jones et al., "Preprocessing strategies to improve MCR analyses of hyperspectral images," *Chemom. Intell. Lab. Syst.* **117**, 149–158 (2012).
27. J. Ohlhausen et al., "Multivariate statistical analysis of time-of-flight secondary ion mass spectrometry images using axsia," *Appl. Surf. Sci.* **231–232**, 230–234 (2004).
28. J. Schoonover, R. Marx, and S. Zhang, "Multivariate curve resolution in the analysis of vibrational spectroscopy data files," *Appl. Spectrosc.* **57**(5), 154A–170A (2003).
29. R. Davis et al., "Accurate detection of low levels of fluorescence emission in autofluorescent background: *Francisella* infected macrophage cells," *Microsc. Microanal.* **16**(4), 478–487 (2010).
30. W. Vermass et al., "In vivo hyperspectral confocal fluorescence imaging to determine pigment localization and distribution in cyanobacterial cells," *Proc. Natl. Acad. Sci. U. S. A.* **105**(10), 4050–4055 (2008).

Matthew S. Graum is a doctoral candidate at the University of New Mexico, School of Engineering in the Department of Nanoscience and Microsystems Engineering. He received his Bachelor of Science degree in biology and his Master of Science degree in nanoscience and microsystems engineering from the University of New Mexico in 2008 and 2012, respectively. His doctoral work involves imaging and quantifying the nanoscale architecture of cell wall components of the pathogenic fungus *Candida*.

Aaron K. Neumann received his PhD in immunology from the University of Pennsylvania, Philadelphia, Pennsylvania in 2005 and has been an assistant professor of pathology at the University of New Mexico, School of Medicine, Albuquerque, New Mexico, since 2012. He investigates host pathogen interactions between innate immunocytes and *Candida* species fungal pathogens, focusing on the biophysics of cell wall organization and receptor signaling using a variety of quantitative fluorescence approaches.

Jerilyn A. Timlin received her PhD in analytical chemistry from the University of Michigan, Ann Arbor, Michigan, in 2000. She is a distinguished member of the Technical Staff in the Bioenergy and Defense Technologies Department at Sandia National Laboratories, Albuquerque, New Mexico. Her research uses fluorescence, Raman, and FTIR spectral imaging, multivariate image analysis, and super-resolution techniques to elucidate complex spatial-temporal relationships of a variety of biomolecules that drive key biological processes.